Follow us @BoneJointRes

Freely available online OPEN ACCESS

BJR

CARTILAGE

Exposure to hypergravity during zebrafish development alters cartilage material properties and strain distribution

E. A. Lawrence,
J. Aggleton,
J. van Loon,
J. Godivier,
R. Harniman,
J. Pei,
N. Nowlan,
C. Hammond

From University of Bristol, Bristol, UK

Aims

Vertebrates have adapted to life on Earth and its constant gravitational field, which exerts load on the body and influences the structure and function of tissues. While the effects of microgravity on muscle and bone homeostasis are well described, with sarcopenia and osteoporosis observed in astronauts returning from space, the effects of shorter exposures to increased gravitational fields are less well characterized. We aimed to test how hypergravity affects early cartilage and skeletal development in a zebrafish model.

Methods

We exposed zebrafish to 3 g and 6 g hypergravity from three to five days post-fertilization, when key events in jaw cartilage morphogenesis occur. Following this exposure, we performed immunostaining along with a range of histological stains and transmission electron microscopy (TEM) to examine cartilage morphology and structure, atomic force microscopy (AFM) and nanoindentation experiments to investigate the cartilage material properties, and finite element modelling to map the pattern of strain and stress in the skeletal rudiments.

Results

We did not observe changes to larval growth, or morphology of cartilage or muscle. However, we observed altered mechanical properties of jaw cartilages, and in these regions we saw changes to chondrocyte morphology and extracellular matrix (ECM) composition. These areas also correspond to places where strain and stress distribution are predicted to be most different following hypergravity exposure.

Conclusion

Our results suggest that altered mechanical loading, through hypergravity exposure, affects chondrocyte maturation and ECM components, ultimately leading to changes to cartilage structure and function.

Cite this article: *Bone Joint Res* 2021;10(2):137–148.

Keywords: Zebrafish, Musculoskeletal, Gravity, Finite element analysis, Extracellular matrix

Article focus

- Altered mechanical loading has been associated with multiple bone and joint pathologies including osteoarthritis and osteoporosis.
- Zebrafish provide an excellent model for musculoskeletal studies as they have many of the cells and tissues found in humans, including a synovial jaw joint which is comparable to human synovial joints.
- Here we use hypergravity to simulate increased mechanical loading and examine how this affects the musculoskeletal system of developing zebrafish.

Key messages

- Short-term hypergravity exposure causes subtle changes to chondrocytes and their surrounding matrix.
- Changes to strain and stress distribution in the lower jaw of larval zebrafish are also observed following short-term hypergravity exposure.

Correspondence should be sent to Elizabeth Anna Lawrence; email: elizabeth.lawrence@bristol.ac.uk

doi: 10.1302/2046-3758.102.BJR-2020-0239.R1

Bone Joint Res 2021;10(2):137–148.

- These alterations could lead to more severe cartilage and bone pathologies over longer exposure periods.

Strengths and limitations

- Strengths of this study include the use of highly specialist equipment, the relevance to human diseases for which mechanical loading is a risk factor, and the range of techniques used to analyze the samples.
- Limitations of this study include the inability to dynamically visualize changes to the musculoskeletal system live due to the large diameter centrifuge setup and the length of exposure to hypergravity; ideally, we would have tested longer exposures but were limited by equipment availability.

Introduction

Mechanical loading of the skeleton occurs during physical activity through muscle contraction and ground reaction forces.[1,2] This loading builds and maintains bone mass, making increased skeletal loading an area of interest in the treatment of osteoporosis.[3] A physiological level of mechanical loading is beneficial to cartilage function in vitro by increasing chondrocyte proliferation and anabolic processes, boosting proteoglycan synthesis.[4-8] In vivo experiments in hamsters,[9] rats,[10] and humans[11] have indicated that moderate exercise has a chondroprotective role, resulting in decreased risk of severe osteoarthritis (OA). In contrast, overloading or reduced loading of joints has a role in cartilage destruction by promoting catabolic pathways. Extreme or abnormal loading (through high impact sports,[12,13] joint misalignment,[14] or surgical interventions such as knee arthroplasty[15,16]) can lead to extracellular matrix (ECM) damage, loss of collagen, chondrocyte cell death, and eventually OA.[17-19]

As mechanical loading is exerted on the skeleton by gravitational forces,[20] many studies on the musculoskeletal system have been carried out across a range of gravity levels. Microgravity has substantial, well-documented effects on the skeleton with decreased bone density observed in humans[21] and fish,[22] and disruptions to skeletal maturation observed in immature mice.[23] Studies on astronauts and cosmonauts following long duration space flight found that 92% had a minimum of 5% bone loss in at least one skeletal site,[24] with weight-bearing regions most affected.[25,26] Sarcopenia is also observed in microgravity, with decrease in muscle volume of around 15% following four to six months in microgravity.[27] While decreased mechanical loading in microgravity has been uniformly associated with disuse bone loss, exposure to hypergravity has been shown to increase or decrease bone depending on the degree of hypergravity. One study exposed mice to hypergravity for 21 days and found that at 2 g, there was an improvement in trabecular bone volume, fewer osteoclasts, and an increase in mineralization.[28] At 3 g they found cortical thinning, more osteoclasts, and a reduced rate of bone formation,[28] supporting the idea that loading is beneficial to a point, after which it becomes deleterious.[29] Zebrafish larvae have been exposed to hypergravity in a large diameter centrifuge (LDC). Aceto et al[30] exposed zebrafish to 3 g and observed increased ossification in the cranial skeleton of larvae exposed to 3 g between five and nine days post-fertilization (dpf).

Another component of the musculoskeletal system sensitive to alterations in biomechanics is cartilage, particularly the articular cartilage of synovial joints. This cartilage has a limited regenerative capacity[31] and is important for absorbing load to protect the underlying bone, ensuring the smooth function of joints.[32] Human bed-rest studies, hind-limb unloading studies in rats, and studies performed on mice exposed to real microgravity have demonstrated that loss of mechanical forces leads to cartilage degradation primarily through proteoglycan loss.[33-36] Cell culture experiments carried out in microgravity also support the observation of cartilage degradation under reduced loading conditions, with cytoskeletal reorganization and ECM composition altered following short exposures.[37-41] In comparison to work on cartilage in unloading conditions, less is known about the effect of hypergravity and increased mechanical loading. One study on cultured chondrocytes showed downregulation of *BMP4* (crucial in collagen type II and aggrecan synthesis)[42] following very short-term cyclic hypergravity exposure during parabolic flight,[43] suggesting that articular cartilage health would be impaired under such loading conditions.

Here, we show that exposure to hypergravity for 48 hours from 3 dpf in zebrafish has no substantial effect on craniofacial cartilage morphology or musculature, but causes significant changes to cartilage material properties, chondrocyte morphology, and ECM organization. We also demonstrate altered strain distribution across the lower jaw following hypergravity exposure, providing an explanation for the cell-level changes. Altogether, this shows that hypergravity exposure in zebrafish larvae between 3 and 5 dpf can induce subtle, but detrimental, changes to cartilage which could become more severe over time.

Methods

Zebrafish husbandry and mutant lines. Zebrafish were maintained as described previously.[44] Experiments were approved by the University of Bristol and the European Space Agency (ESA) and performed in accordance with UK Animals (Scientific Procedures) Act 1986 (ASPA) regulations. ARRIVE guidelines were adhered to and the completed checklist submitted as supplementary material.

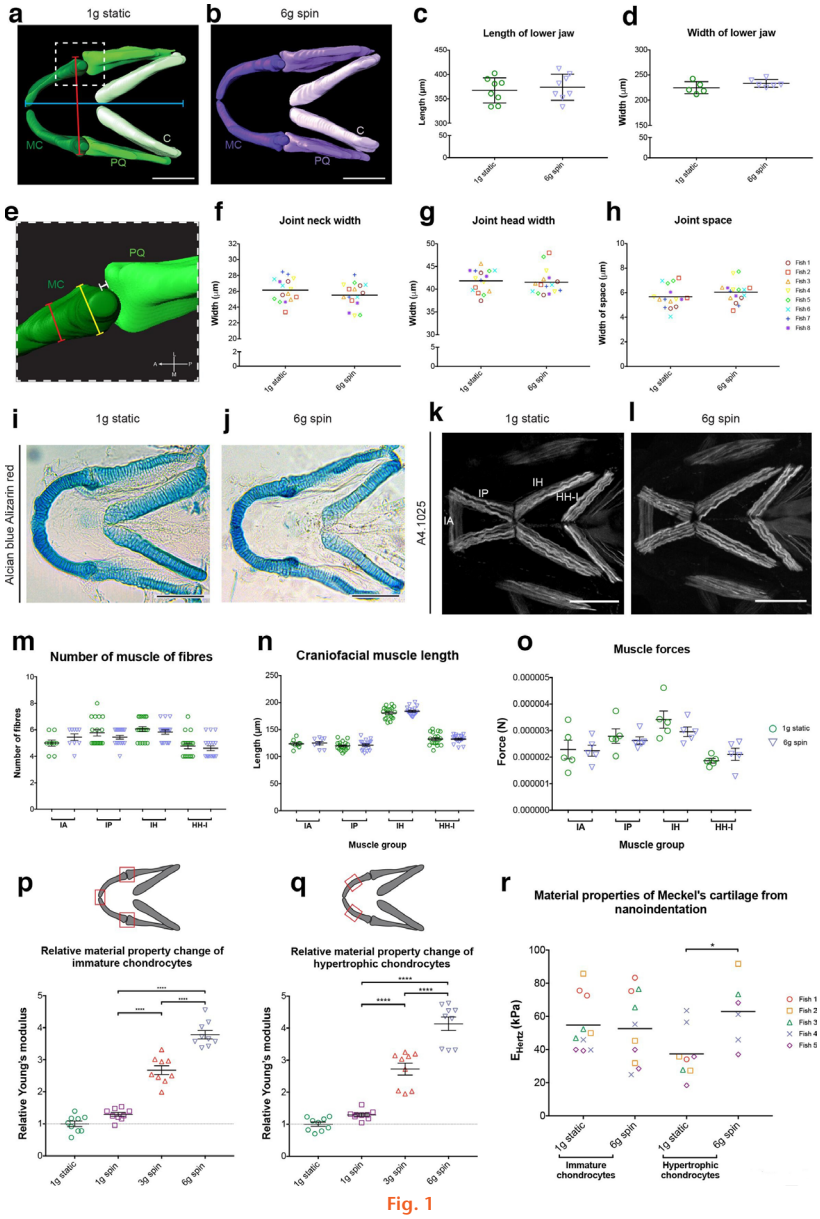

Fig. 1

Lower jaw morphology and musculature are unchanged following hypergravity exposure, but changes to cartilage material properties are observed. a) and b) 3D surface renders from confocal image stacks of lower jaw cartilage in ventral orientation from a) 1 g static and b) 6 g zebrafish at five days post-fertilization (dpf) (MC, Meckel's cartilage; PQ, palatoquadrate; C, ceratohyal). Scale bar: 100 µm. c) and d) Quantification of c) lower jaw length and d) width. Location of measurements shown by red (width) and blue (length) line in Fig. 1a) (n = 8 for all, different symbols = individual fish). e) Close-up image of jaw joint from 1 g static 3D render, position of this region in the lower jaw is shown by white dashed box in Fig. 1a. Orientation compass: A, anterior; L, lateral; M, medial; P, posterior. f) to h) Quantification of f) joint neck and g) joint head width, and h) joint space; location of measurements shown in Fig. 1e. Red line = joint neck; yellow line = joint head; white line = joint space (n = 8 for all). i) and j) Brightfield images of Alcian blue Alizarin red-stained lower jaws from i) 1 g static and j) 6 g conditions. Scale bar = 100 µm. k) and l) Maximum projections of ventral confocal image stacks from 5 dpf j) 1 g static and k) 6 g zebrafish immunostained for myosin (A4.1025) (IA, intermandibularis anterior; IP, intermandibularis posterior; IH, interhyoideus; HH-I, hyohyoideus inferior). Scale bar = 100 µm. m) and n) Quantification muscle fibre m) number and n) length measured from confocal image stacks. Location of muscle groups shown in Fig. 1k). o) Quantification of craniofacial muscle forces. p) and q) Relative Young's modulus (YM) values from atomic force microscopy (AFM) for p) immature and q) hypertrophic chondrocytes from 1 g static and 1 g, 3 g, and 6 g spin zebrafish (n = 3 for all). Location of measurements taken shown in schematic above graphs. r) Material properties determined by nanoindentation in 1 g static and 6 g spin zebrafish. Data are means with standard errors of the mean (SEM). (f) to h) show mean with no SEM), D'Agostino and Pearson test performed for all data, followed by independent-samples *t*-test in c), d), f), g), and h). One-way analysis of variance (ANOVA) performed within muscle groups in m), n), and o), and also in p) and q). Mann–Whitney U test used in r). *p ≤ 0.05, **p ≤ 0.01, ***p ≤ 0.001, ****p ≤ 0.0001.

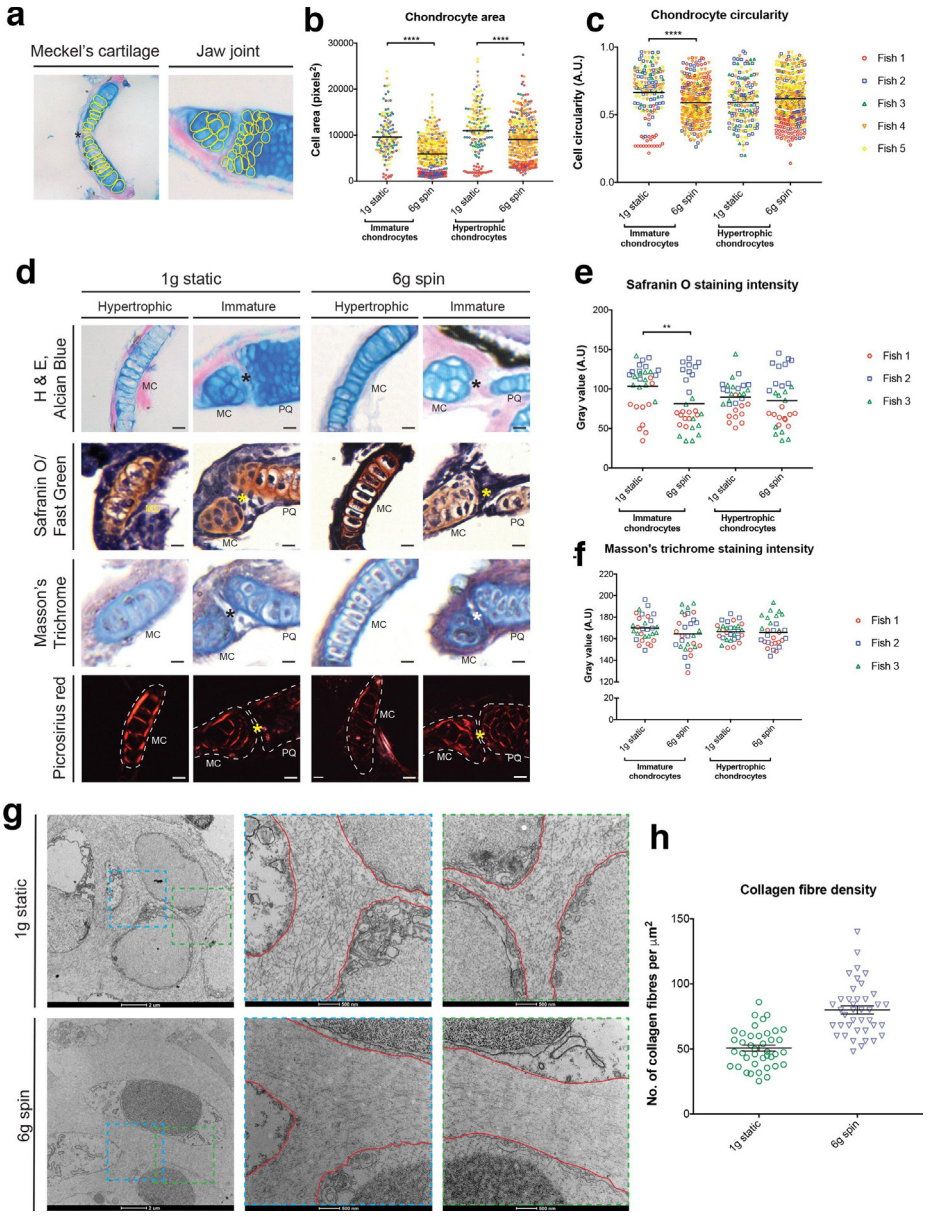

Fig. 2

Subtle changes to chondrocytes and their surrounding extracellular matrix (ECM) occur in areas of altered strain. a) Representative image with chondrocytes included in area and circularity measurements outlined in yellow. Black asterisk, Meckel's symphysis. b) and c) Quantification of b) chondrocyte area and c) circularity (n = 5 for all, colours = individual fish). d) Alcian Blue, Haematoxylin and Eosin; Safranin O and Fast Green; Masson's trichrome; and Picrosirius Red-stained ventral sections in 1 g static and 6 g spin fish. Asterisk = centre of joint; dotted line in Picrosirius Red images = outline of cartilage element from section. Scale bar = 10 μm. MC, Meckel's cartilage; PQ, palatoquadrate. e) and f) Quantification of e) Safranin O and f) Masson's trichrome staining intensity. g) Electron micrographs of hypertrophic chondrocytes in 1 g static and 6 g spin. Dashed areas = higher magnification images displayed in the centre and to the right of the panel; red lines = chondrocyte borders. Scale bars are shown below each image. h) Quantification of collagen fibre density in the ECM of 1 g static and 6 g spin fish (n = 1 for both, each point represents the number of fibres in 1 μm^2). All data are means with standard errors of the mean (SEM). D'Agostino and Pearson normality test performed in b), c), e), and f): followed by Mann–Whitney U test in b) and c), and independent-samples *t*-test in e) and f). *p ≤ 0.05, **p ≤ 0.01, ***p ≤ 0.001, ****p ≤ 0.0001.

Hypergravity experiments. Zebrafish were exposed to hypergravity in the LDC[45] at the European Space Research and Technology Centre (ESTEC) for 48 hours from 3 dpf to 5 dpf. The LDC consists of a central axis linked to two arms. Samples can be placed in six gondolas (which can be set to two different hypergravity levels) plus one central gondola at 1 g to control for rotation and possible related Coriolis accelerations.[46] The larvae were exposed to 3 g and 6 g, with control larvae located at the central axis, and further larvae were maintained at 1 g static (Supplementary Figure aa). In each gondola, four petri dishes (Thermo Fisher Scientific, Waltham, Massachusetts, USA) containing 150 ml of Danieau's solution and < 35 larvae each were

Table I. Muscle forces used for finite element model generation. Values for 1 g static and 6 g spin fish represent 60% of the maximum muscle force calculated for each muscle group in Figure 1o, with the exception of the adductor mandibulae.

Muscle	Muscle forces, N	
	1 g static	6 g spin
Intermandibularis anterior	1.37E-06	1.35E-06
Intermandibularis posterior/ interhyoideus (mean of both)	1.86E-06	1.68E-06
Adductor mandibulae	2.57E-06	2.57E-06

stacked in the centre of an incubator set to a constant temperature of 28°C (Supplementary Figures aa to ad). Larvae were incubated in the dark except during the recording of videos (to monitor survival and swim behaviour during the experiment). Following exposure to hypergravity, one petri dish from each gravity condition was reserved for behavioural studies, with the rest euthanized with MS222 (tricaine methanesulphonate; Sigma-Aldrich, St Louis, Missouri, USA) before fixation in 4% paraformaldehyde (PFA; Thermo Fisher Scientific) or bone fix (3.5% formaldehyde in 40 mM phosphate buffer) for further analysis.

Whole fish measurements. Larvae were mounted in glycerol and imaged on a Leica MZ10F stereo microscope (Leica, Wetzlar, Germany). Head to tail length was measured using the line function in Fiji (Supplementary Figure ae).[47]

Antibody labelling. Immunohistochemistry was performed as previously described.[48] Briefly, larvae were fixed in 4% PFA and dehydrated to 100% methanol (MeOH) for storage, then rehydrated to 1 × phosphate buffered saline + 0.1% triton X-100 (PBST; Thermo Fisher Scientific), permeabilized, and blocked in 5% horse serum prior to incubation in primary antibodies (collagen type II (Abcam ab34712; Abcam, Cambridge, UK) 1:500; A4.1025 (Developmental Studies Hybridoma Bank, University of Iowa, Iowa City, Iowa, USA) 1:500; L-plastin[49] 1:200 (gift from the Martin Lab, University of Bristol); acetylated tubulin (Sigma-Aldrich T6793) 1:200 at 4°C overnight (o/n). Samples were washed three times in PBST, reblocked, and incubated in secondary antibodies (Goat anti-rabbit 555 (Dylight; Thermo Fisher Scientific); Donkey anti-mouse (Thermo Fisher Scientific); Goat anti-chick 647 (Thermo Fisher Scientific); all at 1:500) overnight at 4°C. Where required, larvae were incubated in 5 µg/ml 4′,6-diamidino-2-phenylindole (DAPI) (Invitrogen, Carlsbad, California, USA) for one hour and washed in PBST prior to imaging. Samples were mounted in 0.5% low melting point agarose (Thermo Fisher Scientific) and imaged on a Leica SP5II confocal microscope (Leica) with a 10× or 20× objective.

Alcian blue and Alizarin red staining. Alcian blue and Alizarin red whole mount larval staining was performed as previously described[50] on larvae fixed in 3.5% formaldehyde.

Atomic force microscopy. Atomic force microscopy (AFM) was conducted utilizing a Multi-mode VIII microscope with Nanoscope V controller, operating in a PeakForce control regime (Bruker, Santa Barbara, California, USA). Larval cartilage was investigated in a hydrated state in an ambient environment.[51] Prior to AFM investigation, larvae were fixed in 4% formaldehyde, stained with Alcian blue and Alizarin red (as above), and the lower jaw was dissected in 1% glycerol in phosphate-buffered saline (PBS) to prevent structural changes induced by drying. For measurement of Young's modulus (YM) via quantitative nanomechanical mapping (QNM), RTESPA-150 cantilevers (Bruker) were utilized, having nominal spring constant and tip radii of 5 N/m and 8 nm, respectively. Cantilevers were calibrated via the relative method utilizing a poly(dimethylsiloxane) (PDMS) standard with data fit to a Derjaguin-Muller-Toporov (DMT) model, accounting for the effect of adhesion forces in the standard Hertzian model for indentation. Three fish were investigated for each level of hypergravity exposure. For each fish, three separate 500 nm × 500 nm regions were scanned in both the immature chondrocytes and hypertrophic chondrocytes, six regions in total. Overall, 65,536 measurements were taken per scanned region and their root mean square (RMS) mean calculation recorded for comparison. Data were normalized to values from 1 g static samples to show the relative YMs.[52-57]

Nanoindentation. Larvae were fixed in 4% PFA and stored in 100% MeOH before rehydration to 30% sucrose in PBS. Samples were submerged in 30% sucrose in PBS, and diluted 1:2 in optimal cutting temperature compound (OCT compound) until they sunk. This solution was refreshed for embedding and samples were flash frozen and sectioned in a coronal orientation using an NX70 Cryostat (Thermo Fisher Scientific) at a thickness of 10 µm. Nanoindentation was performed on sections containing the jaw joint and/or Meckel's cartilage using a Chiaro nanoindentation device (Optics11, Amsterdam, The Netherlands). Sections were kept submerged in PBS at room temperature while measurements were taken. A spherical nanoindentation probe with an 8 µm radius and stiffness of 0.49 N/m was used, and tissues were indented to a depth of 1 µm with velocity of 1 µm s^{-1}, with the tip held at a constant depth for ten seconds. The collected curves were analyzed based on Hertzian contact theory for direct comparison with AFM measurements, and the resultant YM E_{hertz} data were calculated assuming the sample's incompressibility. Nanoindentation was performed across all sections containing the joint or Meckel's cartilage, with one measurement collected per region of interest (ROI) in each section. The resulting YM had their means calculated for each region across sections. Nanoindentation was performed on five fish from each of the 1 g static and 6 g spin groups.

Table II. Actual and relative material property values of immature and hypertrophic chondrocytes from atomic force microscopy and nanoindentation, which were used for finite element models. Values represent the mean measurement across samples, and the figure number of the corresponding finite element model is shown in the right-hand column.

Gravity condition	Method	Hypertrophic chondrocytes		Immature chondrocytes		Figure no. of corresponding model
		Actual material property value	Relative material property value	Actual material property value	Relative material property value	
1 g static	AFM	7.7 MPa	1	4.2 MPa	0.51968	Figure 3A
	Nanoindentation	37.39 kPa	1	54.8 kPa	1.46563	Figure 3B
6 g spin	AFM	31.0 MPa	4.13444	15.2 MPa	1.99503	Figure 3A
	Nanoindentation	62.9 kPa	1.68227	52.63 kPa	1.407597	Figure 3B

AFM, atomic force microscopy.

Histological staining. Fixed samples were processed into paraffin, cut in 5 µm sections, deparaffinized, and stained with haematoxylin and eosin (H&E) and Alcian blue, Picrosirius Red, Safranin O/Fast Green, or Masson's trichrome. H&E Alcian blue slides were stained in Erhlic's haematoxylin for five minutes, rinsed, differentiated in acid alcohol and Scott's water, placed in eosin solution for ten seconds, and rinsed and immersed in Alcian blue for 30 minutes. Picrosirius Red slides were immersed in Picrosirius Red for one hour and washed in two changes of acidified water. Safranin O/Fast Green slides were stained with Weigert's iron haematoxylin for ten minutes, washed for a further ten minutes, stained with 0.05% Fast Green solution for five minutes, rinsed in 1% acetic acid, and immersed in 0.1% Safranin O solution for five minutes. Masson's trichrome sections were refixed in Bouin's solution, stained in Weigert's iron haematoxylin then Ponceau Fuschin (Masson's) for five minutes, rinsed, immersed in phosphomolybdic acid solution and counter-stained with Aniline blue both five minutes, and dipped in 1% acetic acid for ten seconds. Following staining, all sections were dehydrated sequentially to 100% industrial methylate spirit (IMS), immersed in xylene for three sets of five minutes, and mounted using DPX mountant (Sigma-Aldrich). Slides stained with Picrosirius Red were imaged under polarized light on a Leica DMI6000 inverted epifluorescence microscope (Leica), and all other slides were imaged on Leica MZ10F stereo microscope.

Measurement of staining intensity from histology slides. To measure the staining intensity of Safranin O and Masson's trichrome, images were opened in Fiji and the segmented line tool was used to draw a line through the ECM surrounding immature and hypertrophic chondrocytes in the jaw region. The plot profile command was then performed to extract the gray value along this line and measurements normalized to the image background to remove white balance discrepancies. This was performed in ten areas of immature and hypertrophic chondrocytes respectively, with measurements recorded from three fish per gravity condition.

Jaw measurements. Confocal image stacks of the lower jaw immunostained for type II collagen were loaded into Fiji,[47] and the line tool, followed by the measure command, were used to take length and width measurements (Figure 1a). 3D jaw renders and joint measurements were executed as previously described in Lawrence et al[51] (Figure 1e) using Amira 6.0 (FEI Company, Hillsboro, Oregon, USA).

Cell circularity and area quantification. Chondrocyte morphology was measured in Fiji from brightfield images of Alcian Blue-stained lower jaw paraffin sections (5 µm thick). The polygon selection tool was used to outline chondrocytes at the joint and intercalation zone of the Meckel's cartilage (Figure 2a), and the area and roundness shape descriptors were collected using the measure command. Cells from the middle of the Meckel's cartilage were classified as hypertrophic and cells from the jaw joint and Meckel's symphysis (black asterisk in Figure 2a) were classified as immature.

Muscle quantifications and calculation of muscle forces. Muscle forces for each muscle group were calculated using methodology from a study by Brunt et al.[58] In brief, muscle fibre number and length were quantified manually in Fiji from confocal images of A4.1025 stained zebrafish and the cross-sectional area of the fibres was calculated using the formula: πr^2. The radii of the fibres were calculated by taking a measurement across each fibre and dividing it by two. To calculate the cross-sectional area of the whole muscle group, the resulting value was multiplied by the number of muscle fibres. This area was multiplied by the maximal force generated per unit area for larval zebrafish skeletal muscles (40 n N/µm^2, from Iorga et al[59]) to give the final force value for the muscle (values obtained for muscle force are listed in Table I).

Finite element analysis. Finite element (FE) models of the lower jaw for 1 g static and 6 g conditions were created from a confocal image stack of a representative experiment specimen. The same cartilage morphology and muscle forces were used for both conditions' models in the absence of significant differences in cartilage and muscle morphology between 1 g static and 6 g

specimens (Figures 1a to 1d, 1k, and 1l). The FE meshes were developed and modelled for jaw opening and closing movements as previously published.[51] Two different versions of the model were created, one for the nanoscale properties derived from AFM and the other using the microscale properties measured by nanoindentation. Relative material properties were derived from AFM and nanoindentation experiments (values used are listed in Table II). For AFM and nanoindentation experiments separately, values were normalized relative to the 1 g static hypertrophic chondrocyte YM. In both experiments, the YM of the joint interzones was set at 0.025% of the 1 g static hypertrophic chondrocyte YM, a markedly lower value than the chondrocyte cells to enable realistic joint movement, and a Poisson's ratio of 0.495. To reflect the respective experimental Poisson's ratios, in the nanoindentation experiment hypertrophic and immature chondrocytes' Poisson's ratios were set at 0.495; in the AFM experiment hypertrophic and immature chondrocytes' Poisson's ratios were set at 0.3. All muscle forces were calculated based on cross-sectional area of the anatomical muscles, with forces reduced to 60% of maximal force (to represent jaw respiratory movement).

Transmission electron microscopy. Transmission electron microscopy (TEM) was performed on 5 dpf larvae fixed in 2.5% glutaraldehyde in 0.1 M sodium cacodylate for one hour at room temperature (RT). These samples were embedded in 3% agarose before being osmium/uranyl acetate stained, dehydrated, and infiltrated with Epon in a Leica EM TP tissue processor using the standard protocol. Prior to sectioning, samples were laterally embedded in 100% Epon and left to harden at 60°C for two days. These blocks were sectioned at a thickness of 70 nm on a Leica EM UC7 RT ultramicrotome using a diamond knife (Diatome, Hatfield, Pennsylvania, USA). Sections were dried overnight before staining in uranyl acetate for five minutes followed by distilled water (dH_2O) washes, five minutes in lead citrate, and a final dH_2O wash. Sections were imaged on a Tecnai 12-FEI 120kV BioTwin Spirit Transmission Electron Microscope (FEI Company).

Analysis of collagen fibre density from TEM images. To analyze collagen fibre density, TEM images were loaded into Fiji and a ROI of 1 μm^2 was drawn in a random location containing ECM. The number of collagen fibres in this ROI was counted using the multipoint tool and this process was repeated for five separate regions per image. Four images were analyzed from two separate sections per fish, with the sections originating from one fish per gravity condition.

Statistical analysis. All statistical analyses were performed in GraphPad Prism version 7.0 (GraphPad Software, San Diego, California, USA) and the null hypothesis was rejected at a p-value of 0.05 or lower. For all datasets, D'Agostino and Pearson tests for normality were performed followed by the appropriate statistical test (independent-samples *t*-test, one-way analysis of variance (ANOVA), or Mann-Whitney U test). Details of statistical tests performed and the 'n' number of the experiment are described further in the figure legends. For all experiments, 'n' refers to an individual fish. Power calculations were performed in PS: Power and Sample Size Calculation software (version 3.1.6),[60] to estimate the appropriate sample size to reject or accept the null hypothesis.

Results

Craniofacial cartilage morphology and musculature are unaffected by hypergravity. Having confirmed there was no delay in larval growth[61] following hypergravity exposure (Supplementary Figure ae), we investigated the effect of increased mechanical loading through hypergravity on developing cartilage, using type II collagen immunostaining (Supplementary Figure b). These analyses did not reveal gross changes to the overall jaw shape, with jaw length and width statistically unchanged in 1 g static and 6 g spin fish (Figures 1c and 1d). Analysis of joint morphology also revealed no significant difference in fish exposed to hypergravity compared to the 1 g controls (Figures 1e to 1h).

Given the association of microgravity with muscle loss,[62,63] we stained larvae with the pan-skeletal myosin marker A4.1025 to visualize muscles in the lower jaw (Figures 1k and 1l). From these images we quantified muscle fibre number, length, and force, with no significant differences in craniofacial muscle seen between zebrafish incubated in normal gravity and at 6 g between 3 and 5 dpf (Figures 1m to 1o).

Material properties are altered in the lower jaw. Changes to mechanical loading have been observed to change skeletal stiffness at both the nano and micro scales.[64] This led us to investigate the relative material properties of lower jaw cartilage using AFM.[52-57] Measurements were taken from areas of immature chondrocytes and hypertrophic chondrocytes (location of measurements shown by schematics in Figures 1p and 1q). In both instances, a positive correlation between the magnitude of gravitational exposure and the measured YM was seen. Fish from 3 g and 6 g had a significantly higher YM than 1 g static or 1 g spin fish (Figures 1p and 1q), with 6 g showing a significant increase in YM compared to 3 g fish. This trend represents a stiffening of the cartilage following hypergravity exposure during development.

Within complex materials, different structures can have a greater influence on stiffness at different length scales. Having used AFM to measure YM at the nanoscale, we employed nanoindentation to investigate material properties of lower jaw cartilage at the micro scale. Measurements from nanoindentation show 6 g spin fish had a significantly higher YM (E_{hertz}) in hypertrophic chondrocytes when compared to 1 g static fish. This pattern of increased stiffness was not seen for immature chondrocytes (Figure 1r).

Exposure to hypergravity affects chondrocyte maturation and behaviour. The impact of hypergravity at a cellular level was evaluated by measuring chondrocyte morphology from Alcian blue-stained lower jaw sections (Figures 2a to 2c). Chondrocyte area was significantly reduced in immature and hypertrophic regions in 6 g spin fish, with immature cells at the joint and Meckel's symphysis showing the largest area reduction (Figure 2b). Immature chondrocytes also showed a significant decrease in circularity (Figure 2c). The regions of most change to cell morphology were colocalized to muscle attachment sites in the mid-Meckel's cartilage and at the jaw joint. This suggests that short exposure to hypergravity alters chondrocyte behaviour, causing cartilage and resulting bones to develop abnormally if maintained in hypergravity for an extended period.

Histological staining reveals subtle changes to the ECM surrounding chondrocytes in areas of altered cell morphology. As increased mechanical loading is associated with higher glycosaminoglycan (GAG) synthesis and decreased ECM secretion,[65] we performed wholemount Alcian blue and Alizarin Red double staining (Figures 1i and 1j) and Alcian Blue, H&E on sections to visualize GAGs throughout the lower jaw (Figure 2d). From bright-field images, we observed no changes to mineralization or GAGs at 5 dpf (Figures 1i, 1J, and 2d), suggesting that secretion of this ECM component is unaffected by altered loading.

The effect of hypergravity exposure on other ECM components was examined using Safranin O, Masson's trichrome, and Picrosirius Red staining on sections of the lower jaw including the joint and Meckel's cartilage. Proteoglycan content and mineralization of the cartilage ECM were visualized with Safranin O/Fast Green staining which marks the cartilage in red, according to the amount of proteoglycan present, and bone in green (Figure 2d). The intensity of this stain was measured, revealing that fish from the 6 g condition had a significantly lower staining intensity in the ECM surrounding immature chondrocytes than 1 g static fish (Figure 2e), corresponding to a reduction in proteoglycan content in the cartilage following hypergravity exposure. No areas of mineralization were seen in the stained sections, so no information on bone formation could be gathered from this technique.

Masson's trichrome staining was used to test whether hypergravity impacted collagen content in chondrocyte ECM (Figure 2d). This stain shows collagen in blue, and measurements of staining intensity showed no significant change to collagen content in the ECM surrounding immature or hypertrophic chondrocytes in 6 g spin fish compared to the ECM in 1 g static fish (Figure 2f). Alongside measuring total collagen in the ECM through Masson's trichrome, Picrosirius Red staining was used to assess the balance of type I and type III collagen fibres in the ECM. Under polarized light, ECM surrounding immature and hypertrophic chondrocytes appeared red/orange (Figure 2d), indicating a predominance of type I collagen fibres over type III (which would give green birefringence). This was unchanged in zebrafish from the 6 g condition (Figure 2d).

Hypergravity causes changes to collagen fibre packing in the ECM. To further explore how the cartilage ECM is affected by hypergravity, TEM was carried out on sections of ear cartilage, which are comparable to regions of hypertrophic chondrocytes in the lower jaw where the most significant change to material properties was seen. From the micrographs, subtle changes to the collagen fibre packing were observed (Figure 2g), with fibres appearing closer together in 6 g spin fish. This observation was strengthened by quantification of fibre density, which revealed a trend for increased fibre density in 6 g spin fish (Figure 2h).

Taken together with histology data, this suggests that hypergravity induces macromolecular changes in the cartilage which give rise to slight changes at the tissue level. If the larvae had been maintained in hypergravity for longer, it is likely that these changes would have become more pronounced, leading to more severe changes to the tissue.

Finite element analyses reveal altered strain distribution in response to hypergravity exposure. To assess whether cell and matrix changes could be correlated with altered strain distribution in the lower jaw, FE models were generated. As no changes in lower jaw morphology or musculature were observed (Figures 1a to 1d, 1o), the same volumetric model and muscle forces were used for both gravity conditions. Different normalized material properties from AFM (Figure 3a) and nanoindentation (Figure 3b) were applied to these models (Table II). From these models, it can be seen that maximum principal strain is more localized to the joint regions in 6 g spin fish with stiffer cartilage, whereas in 1 g static fish strain is distributed over a larger area of cartilage elements (Figures 3a and 3b). Both methods for obtaining material properties of the cartilage show similar change in strain pattern distribution following hypergravity exposure (from 1 g static to 6 g). Similarly, the pattern of von Mises stress is more evenly distributed throughout the jaw in the 1 g static condition, whereas in the 6 g condition stress is localized in regions already experiencing high stress, specifically the regions surrounding the joints (Supplementary Figure c). This pattern is true for both opening and closing movements. The altered patterns of strain observed, in which the largest differences are close to the joint could provide an explanation for the subtle changes to cell maturation, which were more pronounced at the joint, and to changes observed to matrix packing.

Discussion

The impact of microgravity on the musculoskeletal system has been well studied, with exposure to below-Earth gravity linked to muscle loss and decreased bone density. In comparison, relatively little is known about

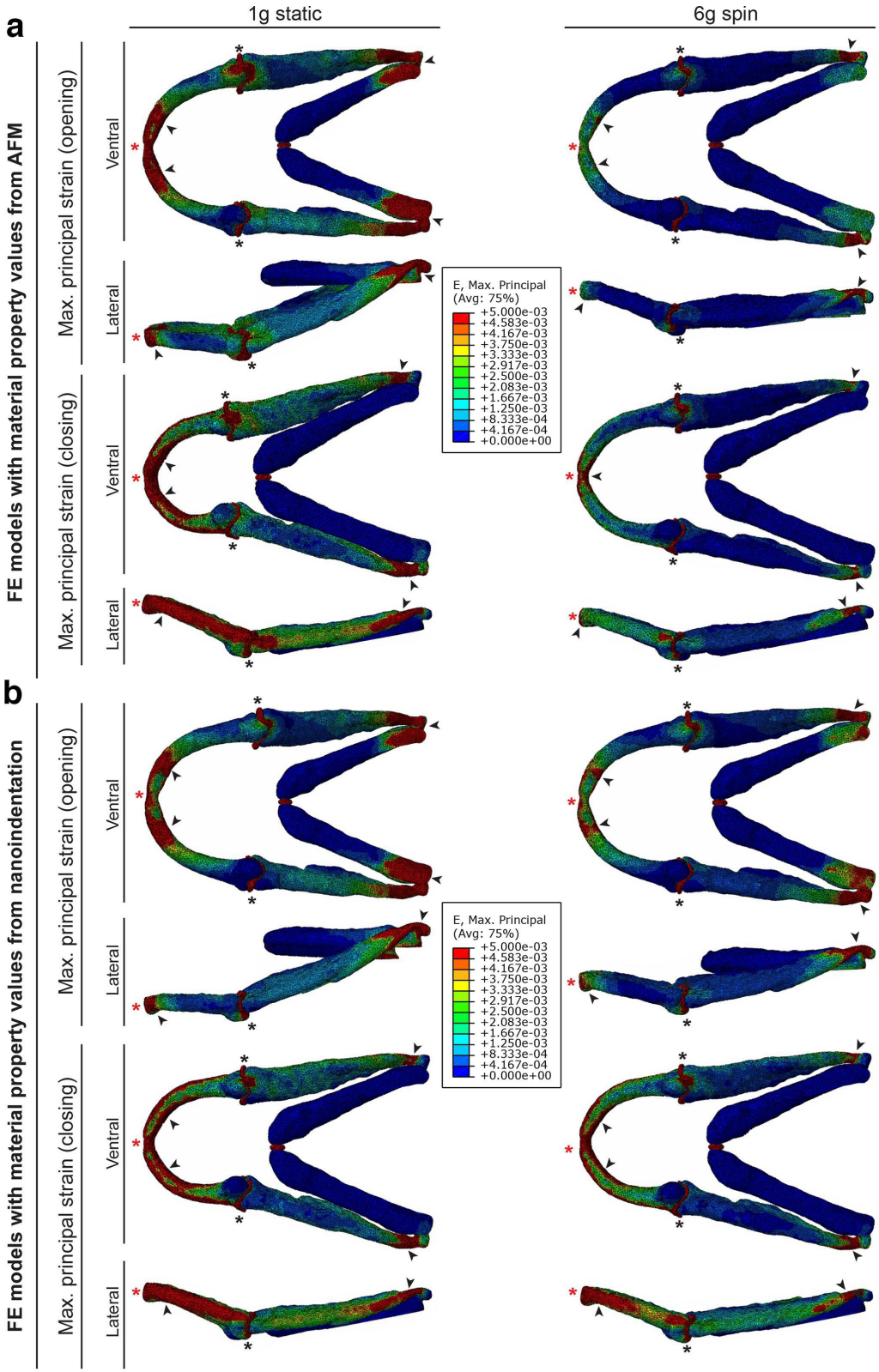

Fig. 3

Altered extracellular matrix (ECM) characteristics could result from altered strain distribution in the lower jaw following hypergravity exposure. a) Finite element (FE) models of maximum principal strain incorporating relative material property values from atomic force microscopy (AFM) in 1 g static and 6 g spin zebrafish. b) FE models of maximum principal strain incorporating relative material property values from nanoindentation in 1 g static and 6 g spin zebrafish. Black arrowheads = areas of high strain; black asterisks = jaw joints; red asterisks = Meckel's symphysis. Ventral and lateral views shown for opening and closing steps in both gravity conditions.

how short-term hypergravity exposure affects the musculoskeletal system. Here, we show that in zebrafish embryos gross cartilage and muscle morphology is unchanged, but cartilage material properties and its resulting biomechanical performance are affected by short-term exposure to hypergravity during development. We also show that hypergravity leads to altered chondrocyte maturation and subtle changes to the surrounding ECM, which may lead to more dramatic changes to the cartilage over time.

Gravity is important for cartilage health as it provides a loading force essential for cartilage homeostasis and prevention of degenerative diseases such as OA.[66-69] Although cartilage morphology and skeletal muscle mass has been shown to be affected by altered loading conditions,[70-73] our data suggest that two days of hypergravity exposure is not sufficient to cause gross morphological changes in larval zebrafish. One explanation for this is the length of exposure being insufficient to induce musculoskeletal remodelling, as previous studies have found that longer exposure to non-Earth gravity leads to more severe musculoskeletal transformations.[21,74] Another explanation for the lack of morphological alterations is that the level of hypergravity was not high enough to induce changes. However, it has previously been shown by Aceto et al[30] that exposure to 3 g between 5 and 9 dpf is sufficient to induce skeletal changes in zebrafish. This indicates that the age at which the zebrafish are exposed to hypergravity is also crucial.[75] Thus, we hypothesize that extending the amount of time larvae spend in hypergravity to include later timepoints key in musculoskeletal development would lead to more dramatic changes.

The hypothesis that more severe cartilage abnormalities would be seen following a lengthier hypergravity exposure is given weight by increased modulus seen in the matrix of zebrafish exposed to both 3 g and 6 g, with the largest increase seen in zebrafish subjected to 6 g. FE analysis revealed that these altered material properties were sufficient to disturb strain pattern in the lower jaw, with the jaw joint and muscle attachment sites showing most change in the craniofacial cartilage elements. In these areas of altered strain, we observed abnormal chondrocyte maturation, which over time would likely give rise to altered joint shape and cartilage morphology.

In conclusion, short-term exposure to hypergravity in early development causes changes to ECM content and organization in zebrafish, which could induce more dramatic structural and morphological changes to the musculoskeletal system over extended exposure periods.

Twitter

Follow E. A. Lawrence @LizzieALawrence
Follow J. Aggleton @jessye_aggleton
Follow C. Hammond @ChrissyLHam

Supplementary material

Supplementary material for this paper includes the ARRIVE checklist and three additional figures: a) setup of experiment in the Large Diameter Centrifuge; b) cartilage morphology following hypergravity exposure; and c) altered extracellular matrix (ECM) characteristics that may result from altered stress distribution in the lower jaw following hypergravity exposure.

References

1. **Usui T**, **Maki K**, **Toki Y**, **et al**. Measurement of mechanical strain on mandibular surface with mastication robot: influence of muscle loading direction and magnitude. *Orthod Craniofac Res*. 2003;6(Suppl 1):163–167.
2. **Lanyon LE**, **Hampson WG**, **Goodship AE**, **Shah JS**. Bone deformation recorded in vivo from strain gauges attached to the human tibial shaft. *Acta Orthop Scand*. 1975;46(2):256–268.
3. **Russo CR**. The effects of exercise on bone. basic concepts and implications for the prevention of fractures. *Clin Cases Miner Bone Metab*. 2009;6(3):223–228.
4. **Lee DA**, **Bader DL**. Compressive strains at physiological frequencies influence the metabolism of chondrocytes seeded in agarose. *J Orthop Res*. 1997;15(2):181–188.
5. **Shelton JC**, **Bader DL**, **Lee DA**. Mechanical conditioning influences the metabolic response of cell-seeded constructs. *Cells Tissues Organs*. 2003;175(3):140–150.
6. **Mauck RL**, **Soltz MA**, **Wang CC**, **et al**. Functional tissue engineering of articular cartilage through dynamic loading of chondrocyte-seeded agarose gels. *J Biomech Eng*. 2000;122(3):252–260.
7. **Sharma G**, **Saxena RK**, **Mishra P**. Differential effects of cyclic and static pressure on biochemical and morphological properties of chondrocytes from articular cartilage. *Clin Biomech*. 2007;22(2):248–255.
8. **Klein-Nulend J**, **Veldhuijzen JP**, **van de Stadt RJ**, **et al**. Influence of intermittent compressive force on proteoglycan content in calcifying growth plate cartilage in vitro. *J Biol Chem*. 1987;262(32):15490–15495.
9. **Otterness IG**, **Eskra JD**, **Bliven ML**, **et al**. Exercise protects against articular cartilage degeneration in the hamster. *Arthritis Rheum*. 1998;41(11):2068–2076.
10. **Galois L**, **Etienne S**, **Grossin L**, **et al**. Moderate-impact exercise is associated with decreased severity of experimental osteoarthritis in rats. *Rheumatology*. 2003;42(5):692–693.
11. **Manninen P**, **Riihimaki H**, **Heliovaara M**, **Suomalainen O**. Physical exercise and risk of severe knee osteoarthritis requiring arthroplasty. *Rheumatology*. 2001;40(4):432–437.
12. **Arendt E**, **Dick R**. Knee injury patterns among men and women in collegiate basketball and soccer. NCAA data and review of literature. *Am J Sports Med*. 1995;23(6):694–701.
13. **Levy AS**, **Lohnes J**, **Sculley S**, **LeCroy M**, **Garrett W**. Chondral delamination of the knee in soccer players. *Am J Sports Med*. 1996;24(5):634–639.
14. **Meireles S**, **Wesseling M**, **Smith CR**, **et al**. Medial knee loading is altered in subjects with early osteoarthritis during gait but not during step-up-and-over task. *PLoS One*. 2017;12(11):e0187583.
15. **Danese I**, **Pankaj P**, **Scott CEH**, **et al**. The effect of malalignment on proximal tibial strain in fixed-bearing unicompartmental knee arthroplasty. *Bone Joint Res*. 2019;8(2):55–64.
16. **MacLeod AR**, **Serrancoli G**, **Fregly BJ**, **Toms AD**, **Gill HS**. The effect of plate design, bridging span, and fracture healing on the performance of high tibial osteotomy plates: an experimental and finite element study. *Bone Joint Res*. 2018;7(12):639–649.
17. **Loening AM**, **James IE**, **Levenston ME**, **et al**. Injurious mechanical compression of bovine articular cartilage induces chondrocyte apoptosis. *Arch Biochem Biophys*. 2000;381(2):205–212.
18. **Torzilli PA**, **Grigiene R**, **Borrelli J**, **Helfet DL**. Effect of impact load on articular cartilage: cell metabolism and viability, and matrix water content. *J Biomech Eng*. 1999;121(5):433–441.
19. **Patwari P**, **Gaschen V**, **James IE**, **et al**. Ultrastructural quantification of cell death after injurious compression of bovine calf articular cartilage. *Osteoarthritis Cartilage*. 2004;12(3):245–252.
20. **Kohrt WM**, **Barry DW**, **Schwartz RS**. Muscle forces or gravity: what predominates mechanical loading on bone? *Med Sci Sports Exerc*. 2009;41(11):2050–2055.

21. **Demontis GC**, **Germani MM**, **Caiani EG**, **et al**. Human pathophysiological adaptations to the space environment. *Front Physiol*. 2017;8:547.
22. **Chatani M**, **Mantoku A**, **Takeyama K**, **et al**. Microgravity promotes osteoclast activity in medaka fish reared at the international space station. *Sci Rep*. 2015;5:14172.
23. **Maupin KA**, **Childress P**, **Brinker A**, **et al**. Skeletal adaptations in young male mice after 4 weeks aboard the International space Station. *NPJ Microgravity*. 2019;5(1):21.
24. **LeBlanc AD**, **Spector ER**, **Evans HJ**, **Sibonga JD**. Skeletal responses to space flight and the bed rest analog: a review. *J Musculoskelet Neuronal Interact*. 2007;7(1):33–47.
25. **LeBlanc A**, **Shackelford L**, **Schneider V**. Future human bone research in space. *Bone*. 1998;22(5 Suppl):113S–116S.
26. **Vico L**, **Collet P**, **Guignandon A**, **et al**. Effects of long-term microgravity exposure on cancellous and cortical weight-bearing bones of cosmonauts. *Lancet*. 2000;355(9215):1607–1611.
27. **LeBlanc A**, **Lin C**, **Shackelford L**, **et al**. Muscle volume, MRI relaxation times (T2), and body composition after spaceflight. *J Appl Physiol*. 2000;89(6):2158–2164.
28. **Gnyubkin V**. Effects of continuous and intermittent hypergravity on skeleton. Saint-Etienne, Université Jean Monnet, 2015. https://tel.archives-ouvertes.fr/tel-01539024/document.
29. **Yokota H**, **Leong DJ**, **Sun HB**. Mechanical loading: bone remodeling and cartilage maintenance. *Curr Osteoporos Rep*. 2011;9(4):237–242.
30. **Aceto J**, **Nourizadeh-Lillabadi R**, **Marée R**, **et al**. Zebrafish bone and general physiology are differently affected by hormones or changes in gravity. *PLoS One*. 2015;10(6):e0126928–0126942.
31. **Karuppal R**. Current concepts in the articular cartilage repair and regeneration. *J Orthop*. 2017;14(2):A1–A3.
32. **Sophia Fox AJ**, **Bedi A**, **Rodeo SA**. The basic science of articular cartilage: structure, composition, and function. *Sports Health*. 2009;1(6):461–468.
33. **Souza RB**, **Baum T**, **Wu S**, **et al**. Effects of unloading on knee articular cartilage T1rho and T2 magnetic resonance imaging relaxation times: a case series. *J Orthop Sports Phys Ther*. 2012;42(6):511–520.
34. **Willey JS**, **Kwok AT**, **Moore JE**, **et al**. Spaceflight-Relevant Challenges of Radiation and/or Reduced Weight Bearing Cause Arthritic Responses in Knee Articular Cartilage. *Radiat Res*. 2016;186(4):333–344.
35. **Ganse B**, **Zange J**, **Weber T**, **et al**. Muscular forces affect the glycosaminoglycan content of joint cartilage. *Acta Orthop*. 2015;86(3):388–392.
36. **Fitzgerald J**, **Endicott J**, **Hansen U**, **Janowitz C**. Articular cartilage and sternal fibrocartilage respond differently to extended microgravity. *NPJ Microgravity*. 2019;5(1):3.
37. **Aleshcheva G**, **Sahana J**, **Ma X**, **et al**. Changes in morphology, gene expression and protein content in chondrocytes cultured on a random positioning machine. *PLoS One*. 2013;8(11):e79057.
38. **Ulbrich C**, **Westphal K**, **Pietsch J**, **et al**. Characterization of human chondrocytes exposed to simulated microgravity. *Cell Physiol Biochem*. 2010;25(4-5):551–560.
39. **Zhang X**, **Li XB**, **Yang SZ**, **et al**. The effects of simulated microgravity on cultured chicken embryonic chondrocytes. *Adv Space Res*. 2003;32(8):1577–1583.
40. **Freed LE**, **Langer R**, **Martin I**, **Pellis NR**, **Vunjak-Novakovic G**. Tissue engineering of cartilage in space. *Proc Natl Acad Sci U S A*. 1997;94(25):13885–13890.
41. **Van Loon JJ**, **Bervoets DJ**, **Burger EH**, **et al**. Decreased mineralization and increased calcium release in isolated fetal mouse long bones under near weightlessness. *J Bone Miner Res*. 1995;10(4):550–557.
42. **Reddi AH**. Bone morphogenetic proteins: from basic science to clinical applications. *J Bone Joint Surg Am*. 2001;83-A Suppl 1(Pt 1):S1–6.
43. **Wehland M**, **Aleshcheva G**, **Schulz H**, **et al**. Differential gene expression of human chondrocytes cultured under short-term altered gravity conditions during parabolic flight maneuvers. *Cell Commun Signal*. 2015;13(1):18.
44. **Westerfield M**. *The zebrafish book. A guide for the laboratory use of zebrafish (Danio rerio)*. 4th ed. Eugene, Oregon: University of Oregon Press, 2000.
45. **Van Loon JJWA**, **Krausse J**, **Cunha H**, **Goncalves J**, **Almeida H**, **Schiller P**. The Large Diameter Centrifuge, LDC, for Life and Physical Sciences and Technology. *Life in Space for Life on Earth*. 2008;553:92.
46. **van Loon JJWA**. The Gravity Environment in Space Experiments. Brinckmann E, ed. *Biology in Space and Life on Earth: Effects of Spaceflight on Biological Systems*. Weinheim: Wiley-VCH Verlag GmbH & Co. KGaA, 2007:17–32.
47. **Schindelin J**, **Arganda-Carreras I**, **Frise E**, **et al**. Fiji: an open-source platform for biological-image analysis. *Nat Methods*. 2012;9(7):676–682.
48. **Hammond CL**, **Schulte-Merker S**. Two populations of endochondral osteoblasts with differential sensitivity to hedgehog signalling. *Development*. 2009;136(23):3991–4000.
49. **Cvejic A**, **Hall C**, **Bak-Maier M**, **et al**. Analysis of WASp function during the wound inflammatory response--live-imaging studies in zebrafish larvae. *J Cell Sci*. 2008;121(Pt 19):3196–3206.
50. **Walker MB**, **Kimmel CB**. A two-color acid-free cartilage and bone stain for zebrafish larvae. *Biotech Histochem*. 2007;82(1):23–28.
51. **Lawrence EA**, **Kague E**, **Aggleton JA**, **et al**. The mechanical impact of *col11a2* loss on joints; *col11a2* mutant zebrafish show changes to joint development and function, which leads to early-onset osteoarthritis. *Philos Trans R Soc Lond B Biol Sci*. 2018;373(1759):20170335.
52. **Nigmatullin R**, **Harniman R**, **Gabrielli V**, **et al**. Mechanically robust gels formed from Hydrophobized cellulose nanocrystals. *ACS Appl Mater Interfaces*. 2018;10(23):19318–19322.
53. **Swift TA**, **Duchi M**, **Hill SA**, **et al**. Surface functionalisation significantly changes the physical and electronic properties of carbon nano-dots. *Nanoscale*. 2018;10(29):13908–13912.
54. **Terry C**, **Harniman RL**, **Sells J**, **et al**. Structural features distinguishing infectious ex vivo mammalian prions from non-infectious fibrillar assemblies generated in vitro. *Sci Rep*. 2019;9(1):376.
55. **Nigmatullin R**, **Gabrielli V**, **Muñoz-García JC**, **et al**. Thermosensitive supramolecular and colloidal hydrogels via self-assembly modulated by hydrophobized cellulose nanocrystals. *Cellulose*. 2019;26(1):529–542.
56. **Melbourne LA**, **Denny MW**, **Harniman RL**, **Rayfield EJ**, **Schmidt DN**. The importance of wave exposure on the structural integrity of rhodoliths. *J Exp Mar Bio Ecol*. 2018;503(1978–2012):109–119.
57. **Gubała D**, **Harniman R**, **Eloi J-C**, **et al**. Multiscale characterisation of single synthetic fibres: surface morphology and nanomechanical properties. *J Colloid Interface Sci*. 2020;571:398–411.
58. **Brunt LH**, **Roddy KA**, **Rayfield EJ**, **Hammond CL**. Building finite element models to investigate zebrafish jaw biomechanics. *J Vis Exp*. 2016(118):54811.
59. **Iorga B**, **Neacsu CD**, **Neiss WF**, **et al**. Micromechanical function of myofibrils isolated from skeletal and cardiac muscles of the zebrafish. *J Gen Physiol*. 2011;137(3):255–270.
60. **Dupont WD**, **Plummer WD**. Power and sample size calculations. A review and computer program. *Control Clin Trials*. 1990;11(2):116–128.
61. **Singleman C**, **Holtzman NG**. Growth and maturation in the zebrafish, Danio rerio: a staging tool for teaching and research. *Zebrafish*. 2014;11(4):396–406.
62. **Martin TP**, **Edgerton VR**, **Grindeland RE**, **et al**. Influence of spaceflight on rat skeletal muscle. *J Appl Physiol*. 1988;65(5):2318–2325.
63. **Caiozzo VJ**, **Baker MJ**, **Herrick RE**, **Tao M**, **Baldwin KM**. Effect of spaceflight on skeletal muscle: mechanical properties and myosin isoform content of a slow muscle. *J Appl Physiol*. 1994;76(4):1764–1773.
64. **Turko AJ**, **Kültz D**, **Fudge D**, **et al**. Skeletal stiffening in an amphibious fish out of water is a response to increased body weight. *J Exp Biol*. 2017;220(Pt 20):3621–3631.
65. **Schröder A**, **Nazet U**, **Muschter D**, **et al**. Impact of mechanical load on the expression profile of synovial fibroblasts from patients with and without osteoarthritis. *Int J Mol Sci*. 2019;20(3):585.
66. **Bader DL**, **Salter DM**, **Chowdhury TT**. Biomechanical influence of cartilage homeostasis in health and disease. *Arthritis*. 2011;2011:979032.
67. **Mellor LF**, **Steward AJ**, **Nordberg RC**, **Taylor MA**, **Loboa EG**. Comparison of simulated microgravity and hydrostatic pressure for chondrogenesis of hASC. *Aerosp Med Hum Perform*. 2017;88(4):377–384.
68. **Penninx BW**, **Messier SP**, **Rejeski WJ**, **et al**. Physical exercise and the prevention of disability in activities of daily living in older persons with osteoarthritis. *Arch Intern Med*. 2001;161(19):2309.
69. **Musumeci G**, **Szychlinska MA**, **Mobasheri A**. Age-related degeneration of articular cartilage in the pathogenesis of osteoarthritis: molecular markers of senescent chondrocytes. *Histol Histopathol*. 2015;30(1):1–12.
70. **Liphardt A-M**, **Mündermann A**, **Koo S**, **et al**. Vibration training intervention to maintain cartilage thickness and serum concentrations of cartilage oligometric matrix protein (COMP) during immobilization. *Osteoarthritis and Cartilage*. 2009;17(12):1598–1603.
71. **Vanwanseele B**, **Eckstein F**, **Knecht H**, **Spaepen A**, **Stüssi E**. Longitudinal analysis of cartilage atrophy in the knees of patients with spinal cord injury. *Arthritis Rheum*. 2003;48(12):3377–3381.
72. **Hinterwimmer S**, **Krammer M**, **Krötz M**, **et al**. Cartilage atrophy in the knees of patients after seven weeks of partial load bearing. *Arthritis Rheum*. 2004;50(8):2516–2520.

73. **Gao Y**, **Arfat Y**, **Wang H**, **Goswami N**. Muscle atrophy induced by mechanical unloading: mechanisms and potential countermeasures. *Front Physiol*. 2018;9:235.

74. **LeBlanc A**, **Schneider V**, **Shackelford L**, **et al**. Bone mineral and lean tissue loss after long duration space flight. *J Musculoskelet Neuronal Interact*. 2000;1(2):157–160.

75. **Franz-Odendaal TA**, **Edsall SC**. Long-Term Effects of Simulated Microgravity and Vibration Exposure on Skeletal Development in Zebrafish. *Stem Cells Dev*. 2018;27(18):1278–1286.

Author information:
- E. A. Lawrence, BSc, PhD Student
- J. Pei, BSc, MPhil Student
- C. Hammond, MBiochem, PhD, Associate Professor in Developmental Genetics School of Physiology, Pharmacology and Neuroscience, University of Bristol, Bristol, UK.
- J. Aggleton, PhD, MSt, BA, PhD Student, School of Physiology, Pharmacology and Neuroscience, University of Bristol, Bristol, UK; School of Anthropology and Archaeology, University of Bristol, Bristol, UK.
- J. van Loon, Dr.-Ing, Scientist, European Space Agency (ESA) Technology Center (ESTEC), TEC-MMG, Noordwijk, The Netherlands; Department Oral & Maxillofacial Surgery/Pathology, Amsterdam Movement Sciences & Amsterdam Bone Center (ABC), Amsterdam University Medical Center Location VUmc & Academic Center for Dentistry Amsterdam (ACTA), Amsterdam, The Netherlands.
- J. Godivier, BSc, PhD Student
- N. Nowlan, BA, BAI, PhD, Reader in Developmental Biomechanics Department of Bioengineering, Imperial College London, London, UK.
- R. Harniman, MSc, PhD, Technician in Atomic Force Microscopy, School of Chemistry, University of Bristol, Bristol, UK.

Author contributions:
- E. A. Lawrence: Performed the laboratory work, Analyzed the data, Designed the study, Drafted the manuscript.
- J. Aggleton: Performed the laboratory work, Analyzed the data, Designed the study, Drafted the manuscript.
- J. van Loon: Supervised the study, Performed the experiments at the Large Diameter Centrifuge.
- J. Godivier: Performed the nanoindentation and resulting analysis.
- R. Harniman: Performed the atomic force microscopy.
- J. Pei: Performed the cell morphology analysis.
- N. Nowlan: Prepared and edited the manuscript.
- C. Hammond: Conceptualized, designed, and coordinated the study, Drafted the manuscript.

Funding statement:
- E. A. Lawrence and J. Aggleton received funding from the European Space Agency (ESA) 'Spin Your Thesis! 2018' program. E. A. Lawrence is also funded by the Wellcome Trust Dynamic Molecular Cell Biology PhD programme. J. Godivier is funded by a PhD studentship from the Anatomical Society. PeakForce atomic force microscopy was carried out with equipment funded by the Engineering and Physical Sciences Research Council (EPSRC) under Grant "Atoms to Applications"; Grant ref. (EP/K035746/1). C. Hammond is funded by Versus Arthritis Senior Fellowship 21937.

ICMJE COI statement:
- The authors declare no competing interests.

Acknowledgements:
- The authors would like to thank Kate Robson-Brown for her invaluable expertise, guidance, and backing throughout the project. They would also like to express their gratitude to the European Space Agency (ESA) Education team, particularly Nigel Savage and Evelien Lageweg, and Alan Dowson at the Large Diameter Centrifuge (LDC) for their support and advice throughout the 'Spin Your Thesis!' campaign. They would like to acknowledge Juan Nunez for his mentorship of E. A. Lawrence and J. Aggleton during the campaign, and the Wolfson Bioimaging Facility for their advice regarding image acquisition. Finally, the authors would like to thank David Labonte and Andrea Attipoe for the use of the Chiaro nanoindentation device and for their helpful assistance.

Ethical review statement:
- Ethical approval for these experiments was provided by the University of Bristol Animal Welfare and Ethics Review Board (AWERB) and the European Space Agency. All experiments were performed on zebrafish aged five days post-fertilization or under. The ARRIVE guidelines were adhered to and a completed ARRIVE checklist has been supplied as supplementary material.